

# Radiation Field Characteristics of Lightning Discharges in the Band 1 kc/s to 100 kc/s

W. L. Taylor

Contribution from Central Radio Propagation Laboratory, National Bureau of Standards, Boulder, Colo.

(Received March 15, 1963)

The groundwave portion of atmospheric waveforms was examined to determine various characteristics of the radiation field from lightning discharges. Sixty-nine representative waveforms were selected from 1,029 atmospherics from 21 thunderstorms in the Oklahoma and North Texas area. The average amplitude and phase spectra, from 1 kc/s to 100 kc/s, are presented for several groups of atmospherics having distinguishable characteristics. Various relationships involving the total radiated energy, peak field strength, first half cycle length, spectral amplitude peak and frequency of spectra peak are presented.

The "normal" type of atmospheric, composing 86 percent of the total, is predominately of positive initial polarity, has a spectrum peak near 5 kc/s and has well defined relationships between the parameters mentioned above. All "other" types of atmospherics are predominately of negative initial polarity, have a spectrum peak from less than 1 kc/s to 18 kc/s and have no well defined relationships between the various parameters.

## 1. Introduction

The return strokes of a lightning discharge emit electromagnetic signals, called atmospherics, that usually attain a spectral peak within the VLF region, i.e., 3 to 30 kc/s, for the radiation field component. The spectra of these signals are very broad, extending from a few cycles per second to as high as 30 Mc/s. Aside from the interference or "noise" from lightning discharges, atmospherics have been utilized by many workers to study the mechanism of thunderstorm electricity, to detect and track thunderstorms, to study whistler mode propagation and to determine VLF and ELF propagation characteristics. It would be exhausting to properly credit all of these accomplishments and also extremely difficult because of much overlapping between the various categories. Examples of literature references covering these subjects are presented at the end of this paper. This paper will be limited to the presentation and description of various characteristics of the radiation field from return stroke lightning discharges. The groundwave portion of atmospherics from sources within a 500 km range was used to minimize propagation effects. Corrections that were applied to the recorded data to overcome limitations of the recording equipment and alteration of the source function by groundwave propagation characteristics are described. The data were separated into various groups by virtue of the wave shape and polarity of individual atmospherics. Characteristics of these groups are described in terms of the total radiated energy, peak field strength, first half cycle length, peak spectral amplitude, and frequency of the spectral peak.

## 2. Collection of Data

Atmospheric waveforms from a large number of lightning discharges in the Oklahoma and North Texas areas were recorded during the spring and summer of 1959. The results presented in this report are from the analyses of the groundwave portion of atmospherics recorded at a site near Lone Wolf, Okla. Selection of data was limited to observation periods occurring after sunset at this site to minimize interference from the first hop skywave. Other National Bureau of Standards recording stations were operated simultaneously with this station to determine the location of individual lightning discharges for the present work and to record data for various VLF propagation studies. These other stations were located at Boulder, Colo.; Salt Lake City, Utah; Palo Alto, Calif.; and Maui, Hawaii.

Each NBS station recorded the broadband vertical electric field of atmospherics, using a vertical antenna; direction of arrival, using a pair of vertical electrostatically shielded loop antennas with broadband equipment; and the time of reception, using timing marks synchronized with the timing signals from stations WWV or WWVH. This information was displayed on multigun oscilloscopes and photographed on continuously moving 35-mm film. The vertical and loop antenna channels included band-pass filters, wideband amplifiers and 24  $\mu$ sec delay lines. Signals that exceeded a selected amplitude from the vertical antenna channel, prior to passing through the delay line were used to activate the oscilloscope displays.

The direction of arrival at each station was determined from a conventional direction-finding (DF) display on one channel of a multigun oscilloscope. This DF channel was activated for approximately 200  $\mu$ sec at the beginning of each atmospheric. The direction of arrival was therefore determined from the initial portion of the signal, which is essentially vertically polarized, with an accuracy of about  $\pm 2^\circ$  for each station.

The time of reception was determined to an accuracy of about  $\pm 1$  msec. The limitation in timing accuracy resulted from a relatively slow recording film speed of 3.3 in./sec, and from the necessity of determining the correction for propagation time of the signals from the standard time stations to the recording sites.

Atmospherics from individual lightning discharges were identified on the photographic records from each station by virtue of their times of reception and directions of arrival. The location of each discharge was determined by triangulation, using the direction of arrival indicated at each station.

The recording sensitivities and triggering amplitudes were selected for each station to accommodate atmospherics originating within about a 500-km radius from the Lone Wolf site. The Lone Wolf equipment was adjusted to trigger from signals of plus and minus polarity with amplitudes equal to or greater than about 0.2v/m. The average distance to the atmospheric sources selected for this study was approximately 350 km.

The amplitude and phase as a function of frequency for the Lone Wolf vertical antenna channel are shown in figure 1. These curves represent the transfer characteristics for a transient signal presented on the cathode-ray tube of the multigun oscilloscope relative to the free space vertical electric field at the antenna. Calibration was performed by inserting a voltage into a dummy antenna driving the cathode follower at the base of a 23-ft vertical antenna. The amplitude response was adjusted by high pass and low pass filters and sloped to 6 db points at 500 c/s and 100 kc/s. The phase response was zero from 4 kc/s to about 50 kc/s, leading by 55 deg at 1 kc/s and leading by about 20 deg at 100 kc/s. This phase was computed for transient signals and therefore does not show the effect of an 8.6 degree phase lag per kilocycle

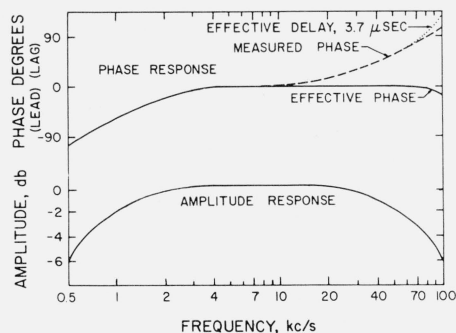


FIGURE 1. Transfer characteristics of the vertical antenna channel.

produced by the 24  $\mu$ sec delay line. The dashed curve shows the phase lag produced by the low pass filter and other electronic components. This approximates an effective delay of 3.7  $\mu$ sec shown by the dotted curve. It is the difference between the measured phase and the phase lag from a 3.7  $\mu$ sec effective delay that gives the effective phase response for a transient signal.

### 3. Analyses

#### 3.1. Data Selection and Classification

Twelve observation periods of 3 min each were selected for this study. The total number of atmospherics recorded from all distances was 2,763, or an average of one every 0.78 sec. Of this total, 1,029 atmospherics, or one every 2.1 sec, originated from 25 thunderstorm areas within about 500 km of the Lone Wolf site. The average number of atmospherics per minute from each thunderstorm area was 4.6, with values ranging from 2.6 to 11.0. This latter value was obtained during severe activity centered some 300 to 400 km from the site.

Examples of atmospheric waveforms are shown in figure 2. These are reproduced on the same time base but with individual amplitude scales. Distances to the source are indicated and the first hop skywave arrival time is shown by the arrow marked "s". Zero  $\mu$ sec on the time base corresponds to the beginning of the VLF portion of the atmospheric; i.e., the return stroke of the discharge. The effect of the delay line used in the waveform signal channel of the recording equipment is evident in the initial part of each trace showing the background or noise preceding the main waveform. Some of these small deflections may be part of the radiation from a stepped leader or dart leader process. The higher frequency oscillations superimposed on the groundwave records are probably produced in part by variations in the return stroke current-moment. A number of workers have reported on these phenomena [Lutkin, 1939; Malan and Schonland, 1951; Norinder, 1952; Pierce, 1955a and 1955b; Kitagawa and Brook, 1960].

The groundwave and skywave portions of the waveforms shown in figure 2 are completely separated except for the waveform in figure 2b. The time interval between the reception of the groundwave and first hop skywave pulses is a function of the distance to the source and the height of the ionospheric reflection layer, in this case, the *D*-region. The extent of interference between these pulses is determined by the time interval between reception and the pulse length of the groundwave. As a consequence of this, probably about 100  $\mu$ sec of the second half cycle of the groundwave shown in figure 2b was obscured. Prior to performing the spectral analyses of the groundwave pulses, under conditions represented by this sample waveform, the trailing edges were reconstructed as indicated by the dashed line. The differences that exist between the reconstructed and actual waveforms are believed to be small. Therefore, the error in the present analyses is not considered to be serious.

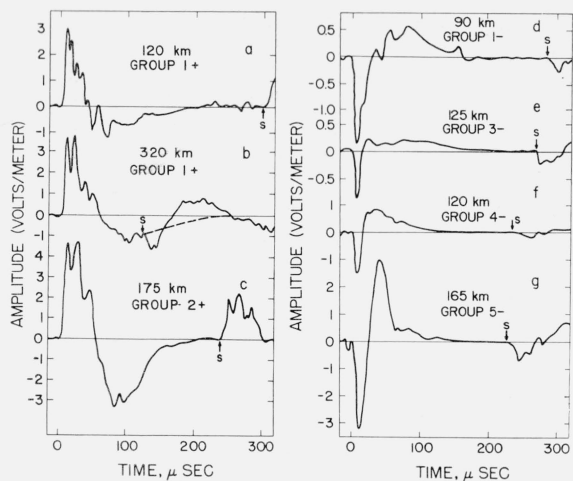


FIGURE 2. Examples of atmospheric waveforms.

During the process of studying the waveform data of the recording site from sources within about 500 km, it became evident that waveforms with persistent characteristics were observed during various observation periods. The author has selected six main groups into which all of the observed waveforms could be placed. Each of these groups was subdivided into two groups determined by the initial polarity of each waveform. It should be emphasized that this grouping is not intended to be a new system of classification of atmospheric waveforms. Some of these groups may be redundant with regard to the physical properties of lightning strokes. Atmospherics placed in groups 1 and 2 might well be considered as a single "normal" type group. Also, the atmospherics placed in groups 3 and 4 are similar in many respects, and could be considered as a single group. These groups were chosen only for the purposes of reporting the data and referencing within the paper.

Group 1-positive, represents those waveforms most often observed from lightning strokes. Representatives of this group are shown in figure 2a and 2b. This group is characterized by positive initial polarity; an average zero axis crossing time or first half cycle length, of 55  $\mu$ sec; a long second half cycle that is approximately 30 percent of the first half cycle amplitude; and often higher frequency perturbations along the waveform. Group 1-negative, represented by the waveform in figure 2d, is characterized by negative initial polarity, and otherwise is similar to group 1-positive.

An example of group 2-positive is shown in figure 2c. The second half cycle of waveforms in this group reaches a peak amplitude about 60 percent that of the first half cycle. Otherwise, this group is similar to group 1-positive. Characteristics of waveforms in group 2-negative are the same as for group 2-positive except the initial polarity is negative.

These first two main groups contain about 86 percent of all atmospherics recorded at ranges of less than about 500 km. In the remaining analyses,

atmospherics in these groups will be referred to as normal atmospherics.

Characteristics of waveforms in groups 3, 4, and 5 are similar in many respects. The samples shown in figure 2e, 2f, and 2g have first half cycle lengths much shorter than observed from normal atmospherics, and the waveforms are usually free of large higher frequency perturbations. Group 3-negative is characterized by an extremely small second half cycle amplitude. The second half cycle of group 4-negative is about 50 percent that of the first half cycle. Group 5-negative is characterized by a very large second half cycle, about equal in amplitude to the first half cycle. The positive counterparts of groups 3, 4, and 5 are similar in shape except for a reversal in polarity.

A summary of the number of atmospherics and the percentage of positive polarity waveforms for each group and for combinations of groups is presented in table 1.

TABLE 1. Number of atmospherics in each group.

GROUP	NO.	TOTALS	%+	TOTALS	%+	TOTAL	%+
1+	784	831	94	883	94	1029	82
1-	47						
2+	43	52	83	131	10	1029	82
2-	9						
3+	5	57	8.8	15	20	1029	82
3-	52						
4+	8	74	11	15	20	1029	82
4-	66						
5+	3	15	20	15	20	1029	82
5-	12						

Only 69 atmospheric waveforms were selected from the total of 1,029 waveforms recorded from atmospherics within a 500 km radius of Lone Wolf. It was first of all necessary to limit the number to be used for spectral analysis because of the extensive labor required for the processing and scaling and the considerable expense for the electronic computer analysis. Therefore, the author decided to select not over 10 percent of the total for further analysis. The first requirement for each waveform was that it be free from obvious interference, such as signals from other lightning discharge processes and from the first hop skywave. Discharge processes such as stepped leaders, dart leaders, intercloud and intracloud discharges, etc., from relatively near (50 km) thunderstorms, produced a considerable amount of interference or background noise during some of the observations. First hop skywave interference was more severe at the greater ranges and therefore very few waveforms from lightning strokes at distances greater than about 400 km were selected. The elimination of waveforms with a large amount of interference resulted in reducing the number of analyzable waveforms to about 18 percent of the total number. All remaining waveforms in groups 2, 3, 4, and 5 were

analyzed. To complete the selection, every fifth lightning discharge from each thunderstorm area were chosen. Then all waveforms with group 1 characteristics, radiated from the lightning strokes comprising the chosen discharge, were analyzed.

It is reasonable to conclude that the present selection is representative of the 1,029 atmospherics recorded for this study, and indeed representative of all atmospherics originating from this particular locale. Of course it must be realized that small changes in the relationships of the various parameters might result from the selection of waveforms other than those chosen for spectrum analysis in the present case.

Another classification, group 6, is that of whistler producing atmospherics. These atmospherics are characterized by large amplitudes and a smooth oscillatory nature after the first few hundred microseconds of the waveforms. [Helliwell, Jean, and Taylor, 1958; Hepburn, 1959; Norinder and Knudsen, 1961.] Several waveforms of this type were recorded from sources within 500 km distance. These were not included in the present study because of the long pulse length, low frequency characteristics of the source and interference from the first hop skywave.

### 3.2. Spectral Computations

The Fourier spectrum of the vertical electric field of an atmospheric can be represented by the integral:

$$E(\omega, d) = \int_0^{\tau} G(t, d) \cdot e^{-i\omega t} dt \quad (1)$$

where  $\omega$  is the angular frequency ( $2\pi f$ ),  $d$  is the distance in kilometers,  $t$  is the time in seconds and the function  $G(t, d)$  is the instantaneous value of the field in volts per meter. Integration starts at time  $t=0$  and ends at  $t=\tau$ , since

$$G(t, d) = 0 \text{ for } t \leq 0 \text{ and for } t \geq \tau. \quad (2)$$

Now (1) can be written in the form

$$E(\omega, d) = |E(\omega, d)| \cdot e^{-i\phi(\omega, d)}. \quad (3)$$

The function  $|E(\omega, d)|$  is the amplitude spectrum and the function  $\phi(\omega, d)$  is the phase spectrum as a function of frequency ( $2\pi f$ ) and distance.

The complex spectral component of 69 atmospherics was calculated at intervals of 1 kc/s from 1 to 30 kc/s, every 2 kc/s from 32 to 50 kc/s, and every 5 kc/s from 55 to 100 kc/s, on an electronic computer. The spectrum of each atmospheric pulse was corrected for recording equipment response and normalized to a common distance of 1 km as a matter of convenience for other studies utilizing atmospherics.

This normalization to the 1 km value not only included the inverse distance relationship for amplitude; i.e.,  $|E(\omega, d)| \propto 1/d$  (this assumes a flat earth, but is sufficiently accurate at short ranges), but also included the effects of propagation on the amplitude and the phase of the signal. The amplitude and phase components of groundwave propagated signals

have been computed by Johler, Kellar, and Walters [1956]; Wait and Howe [1956]. Applying the computations for amplitude and phase, reported in the above references, to the spectra of each atmospheric pulse, it was possible to approximate the true amplitude spectrum and phase spectrum of the radiation component at 1 km. The amplitude attenuation and phase variation for a given frequency is of course a function of distance and ground conductivity. It was assumed for this study that the effective ground conductivity in the Oklahoma and North Texas area was  $10^{-2}$  mhos/m [Jordan, 1950].

The "corrected" 1 km value of the amplitude normalization factor can be defined as the amplitude at 1 km divided by the amplitude at the propagation distance for each atmospheric and for each frequency of the amplitude spectrum. These amplitudes were derived from the amplitude versus distance curves of Wait and Howe [1956]. These theoretical curves include the effects of finite ground conductivity and of normal atmospheric refraction. The amplitude spectrum computed for each atmospheric was multiplied by the corrected 1 km normalization factor to determine, at each frequency, the spectral amplitude of the radiation component at 1 km.

An "uncorrected" 1 km value of the amplitude normalization factor can be defined simply as the propagation distance in kilometers.

Differences between the amplitude spectra referred to 1 km using corrected and uncorrected normalization factors were small for all frequencies (1 to 100 kc/s) at the shorter ranges (100 to 200 km), amounting to less than 15 percent of the uncorrected value. As the propagation distance increased, these differences became more pronounced. At a range of 500 km, for example, the differences between the corrected and uncorrected values of the 100 kc/s component of the spectrum amounted to about 50 percent of the uncorrected amplitude spectrum value.

As indicated in (1), the integration time started at time  $t=0$ . Time  $t$  was therefore the instant when energy first arrived at the recording site from the stroke. The propagation of energy corresponds to the group velocity. In free space, the group velocity and the phase velocity are equal to the universal constant,  $c$ ; i.e.,  $\approx 3 \times 10^8$  km/sec. The group and phase velocities, however, are less than  $c$  for ground-wave propagation. The group velocity, for purposes of this study, was assumed to be that of the 100 kc/s component of each waveform corresponding to the initial arrival of energy. Theoretical values for the group velocity, in the form of delay time (in  $\mu\text{sec}$ ) relative to free space, have been computed by Johler, Kellar, and Walters [1956]. Theoretical values for the phase velocity, in the form of degrees (phase lag) relative to free space, have been computed by Wait and Howe [1956].

The phase spectrum  $\phi(\omega, d)$ , for each atmospheric was corrected by subtracting the phase value resulting from the phase velocity at each frequency less the group velocity at 100 kc/s. It should be noted that these phase values were a function of finite ground conductivity and distance as well as frequency. These corrections to the recorded phase spectra were

relatively small, amounting to less than 30 degrees for frequency components between 1 kc/s and 100 kc/s and for distances from 100 km to 500 km.

A relatively large error in the spectra of the recorded waveforms resulted from the transfer characteristics of the equipment. Therefore, the spectra were corrected by the corresponding response presented in figure 1. As an example: at 1 kc/s, the amplitude was increased by 2 db and the phase increased by 55°; at 2 kc/s the amplitude was increased by 0.4 db and the phase increased by 19°; and so on.

The spectra presented in figures 3 through 7 are averages of various atmospheric groupings. The amplitude spectrum,  $|E(\omega)|$ , in micro-volt-seconds per meter ( $\mu\text{vsec/m}$ ) versus frequency in kilocycles per second represents the amplitude of the radiation component of the electromagnetic field at a distance of 1 km. It should be noted that actual recordings at this distance would involve extremely large static field components. Also, it should be realized that radiated energy is proportional to the square of the spectral amplitude component at each frequency. The phase spectrum,  $\phi(\omega)$ , in degrees versus frequency represents the phase of the radiation component. Positive degrees indicate a phase lag. The electronic computer was coded such that the analysis of a sine wave, where  $t=0$  corresponds to the time the sine wave crosses the zero axis moving in a positive direction, will result in a phase of zero degrees. Also, the analysis of a cosine wave, where  $t=0$  corresponds to the time a sine wave reaches the maximum positive excursion, will result in a phase of minus 90 deg.

Maximum deviation of the spectral values of individual atmospheric in each group is indicated by the dashed lines on either side of the average spectrum. These values were determined only at frequencies of 1, 2, 5, 10, 20, 50, and 100 kc/s. It should be noted that the maximum deviation of a particular group depends on the sample size or total number in the group. Therefore, it would be expected that the maximum deviation would increase somewhat with a larger sample size.

Computing these values for the amplitude spectra involved normalizing the individual spectrum to the average total radiated energy value for each group. This was accomplished by multiplying the spectral components computed at the above frequencies by the quantity  $|E(\omega)|_p^{\text{ind}} \div |E(\omega)|_p^{\text{ave}}$ . The  $|E(\omega)|_p$  is the value of the amplitude spectrum normalized to 1 km, at its maximum or peak value. The superscripts ind and ave denote respectively the spectral peak for individual atmospheric and for the average of the group as determined by the relation

$$E_T = 9 \times 10^{-4} |E(\omega)|_p^{1.8} \quad (4)$$

where  $E_T$  is total radiated energy. This relation, obtained from the data presented in figure 11, will be covered in greater detail later. The average total radiated energy for each group is indicated on each figure.

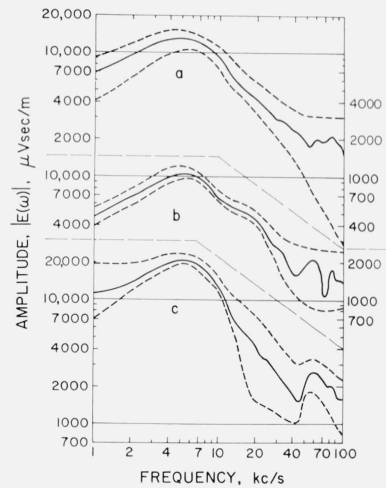


FIGURE 3. Average amplitude spectra.

- (a) Group 1-positive, ave  $E_T=61,000$  j.
- (b) Group 1-negative, ave  $E_T=35,300$  j.
- (c) Group 2-positive, ave  $E_T=97,000$  j.

Maximum deviations as shown on the phase spectra did not involve any further computations or normalizations. Here again, the maximum deviations would tend to increase for a larger number of samples.

The amplitude spectra in figure 3 are averages for the normal type atmospheric. The group 1-positive spectrum is shown in figure 3a, group 1-negative spectrum in figure 3b, and group 2-positive in figure 3c. Representative waveforms of these were presented in figures 2a, 2d, and 2c, respectively. The frequency of the maximum amplitude of the group 1-positive spectrum was at 5 kc/s. The spectra of all atmospheric in this group reached a peak between 4 kc/s and 7.5 kc/s. Similarly, the peak of the group 1-negative spectrum was at 5.5 kc/s, and the range of values within the group was between 5 kc/s and 6 kc/s; the peak of the group 2-positive spectrum was at 5 kc/s, and the range of values within the group was between 4 kc/s and 6 kc/s. Marked similarity was observed between the spectra of individual atmospheric in the normal groups and consequently between the group averages. Perturbations in the higher frequency components are probably produced by variation in the return stroke current mentioned earlier.

The average amplitude spectra for group 3-minus, group 4-minus and group 5-minus are presented in figures 4a, 4b, and 4c and correspond respectively to the representative waveforms shown in figures 2e, 2f, and 2g. The spectra for groups 3 and 4 are very similar and undoubtedly result from similar discharge characteristics. Although the frequency at which the average amplitude reaches a peak for these two groups is apparently less than 1 kc/s, the spectral peak of individual atmospheric extends to 6.5 kc/s for group 3 and 5.5 kc/s for group 4.

Presented in figure 4c, is the average amplitude spectrum for group 5-negative, represented by at-

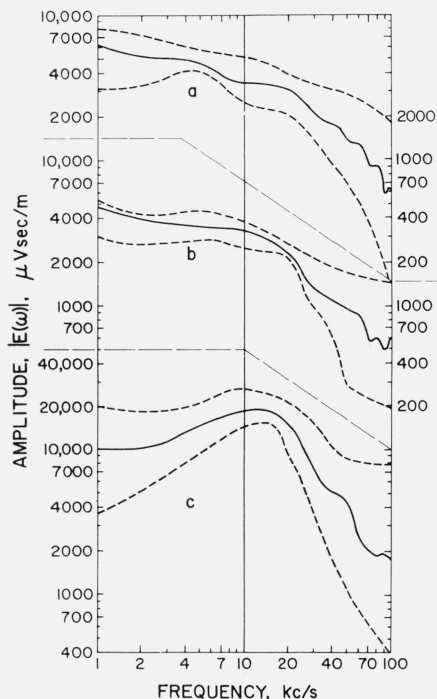


FIGURE 4. Average amplitude spectra.

- (a) Group 3-negative, ave  $E_T=22,100$  j.
- (b) Group 4-negative, ave  $E_T=6,600$  j.
- (c) Group 5-negative, ave  $E_T=225,000$  j.

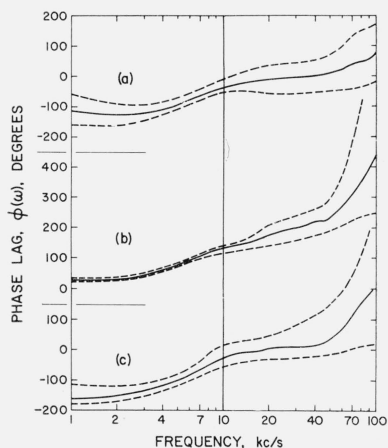


FIGURE 5. Average phase spectra.

- (a) Group 1-positive.
- (b) Group 1-negative.
- (c) Group 2-positive.

atmospherics similar to the sample in figure 2g. Atmospherics in this group are usually of larger amplitude than other types. The average spectrum peaks at about 12 kc/s with peak spectral values of individual atmospherics in the group ranging from 9 kc/s to 17.5 kc/s. The spectral amplitude, above 20 kc/s, decreases approximately as the negative 1.5 power of the frequency. This is greater than the rate of decrease observed for the other groups which

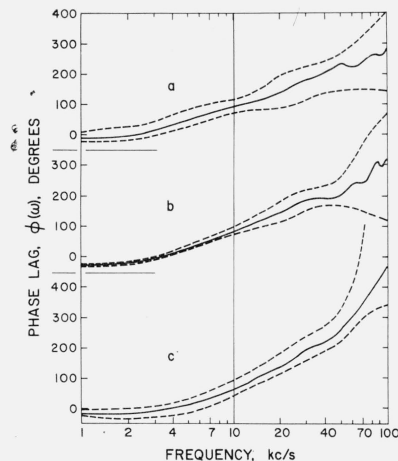


FIGURE 6. Average phase spectra.

- (a) Group 3-negative.
- (b) Group 4-negative.
- (c) Group 5-negative.

is proportional to about the negative unity power of frequency.

The phase spectra for the normal atmospheric are given in figure 5a for group 1-positive, 5b for group 1-negative, and figure 5c for group 2-positive. Maximum deviations in phase of individual atmospherics are indicated by the dashed lines. The phase curves in figures 5a and 5c are for normal atmospheric with initial positive polarity. It should be noted that the phase is leading by approximately  $90^\circ$  at the frequency for which the amplitude frequency reaches its maximum value, see figures 3a and 3c. Likewise, the phase in figure 5b, negative initial polarity, is lagging by approximately  $90^\circ$  at the frequency of peak amplitude. The phase above 10 kc/s closely approximates a linear function of frequency. Computed from figures 5a, 5b, and 5c, respectively, the phase lag per kilocycle is about 1 deg, 3 deg, and 2 deg. At frequencies below 10 kc/s the phase also approximates a linear function of frequency, with respective values of 10 deg, 10 deg, and 15 deg per kilocycle.

The phase spectra for groups 3, 4, and 5, negative polarity atmospheric only, are presented in figures 6a, 6b, and 6c. The corresponding amplitude spectra were given in figures 4a, 4b, and 4c. For groups 3 and 4, the phase is lagging by about  $90^\circ$  at 10 kc/s. Contrary to the phase and amplitude relationships of other groups, this does not correspond to the peak amplitude frequency. The phase above 10 kc/s, for these two groups, closely approximates a logarithmic function of frequency (phase  $\approx 200 \log$  of freq. in kc/s-100). The phase below 10 kc/s tends to vary linearly with frequency, at a rate of about 12 deg per kilocycle. For group 5, see figure 6c, the phase lags by about  $90^\circ$  at the peak amplitude frequency, as was the case for normal atmospheric of negative polarity. The variation of phase is approximately linear with frequency: about 7.5 deg per kilocycle at frequencies below 30 kc/s and about 3.5 deg per kilocycle at frequencies above 30 kc/s.

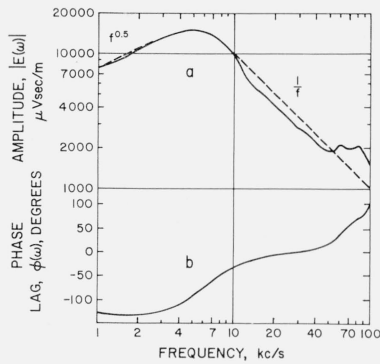


FIGURE 7. Average spectra, normal atmospherics, normalized to 1 km.

(a) Amplitude  $|E(\omega)|$ .  
 (b) Phase  $\phi(\omega)$ .

The average amplitude spectrum for the normal positive initial polarity atmospherics is presented in figure 7a. The amplitude component reaches a peak at 5 kc/s. At frequencies below the peak, the spectral amplitude is proportional to the 0.5 power of the frequency; and at frequencies higher than the peak, the spectral amplitude decreases approximately as the negative unity power of frequency.

Presented in figure 7b, is the average phase spectrum for the normal positive polarity atmospherics. The phase at 5 kc/s, the peak spectral amplitude, is leading by about  $90^\circ$ . The variation of phase is approximately a linear function of frequency. At frequencies up to 10 kc/s, the phase increases, i.e., becomes more lagging, at a rate of about 12 deg per kilocycle; and above 10 kc/s the phase increases about 1.5 deg per kilocycle.

The average amplitude spectrum of the normal negative polarity atmospherics should have the same characteristics as that for the positive polarity atmospherics. The average phase spectrum for the negative polarities should be also very similar to that for the positive polarities except that the phase will be increased by  $180^\circ$  at all frequencies.

The average spectra presented in figure 7 were computed from the analyses of 47 selected normal type waveforms. They represent 86 percent of all atmospherics recorded at distances less than about 500 km.

### 3.3. Relationships

There are a number of parameters involving the wave shape and the analyses of atmospherics that can be compared in an effort to better understand the phenomenon. It is the purpose of this section to present the relationships found to exist between various readily measurable parameters.

The electromagnetic radiation from a lightning discharge contains a very small amount of the total available energy. Only about 1 part in  $10^5$  or  $10^6$  is partitioned into radio energy. For the purpose at hand, it is desired to calculate the radio energy radiated into the earth's atmosphere by lightning

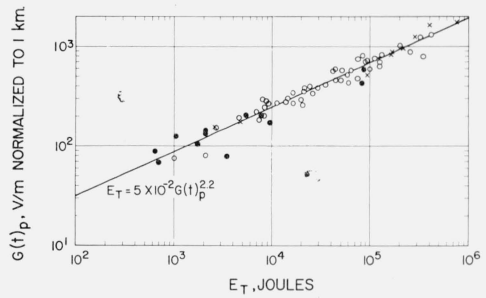


FIGURE 8. Pulse amplitude versus total radiated energy.

discharges. The energy density,  $E_d$  in joules per square meter, of the transient  $G(t, d)$  is represented by

$$E_d = \frac{1}{120\pi} \int_0^\tau G(t, d)^2 dt \quad (5)$$

where  $G(t, d)$  and  $\tau$  were defined in (1) and (2).

Assuming that the source can be represented by a vertical dipole, the radiation component of the vertical electric field is proportional to the cosine of the angle of elevation above the horizontal plane. The total energy in the radiation term,  $E_T$ , in joules, radiated into the atmosphere can be obtained by integrating the energy density,  $E_d$ , over the surface of the radiation pattern of the source. Therefore,

$$\begin{aligned} E_T &= \int_0^{2\pi} \int_0^{\pi/2} E_d r^2 \cos^3 \theta d\theta d\varphi \\ &= 4/3\pi r^2 E_d \end{aligned} \quad (6)$$

where  $r$  is the distance in meters from the source to the observation point,  $\theta$  is the angle of elevation measured from the horizontal, and  $\varphi$  is the angle measured in the horizontal plane.  $E_T$  will be referred to as the total radiated energy in joules.

There is a wide variation in the characteristics of individual groundwave pulses. Atmospherics from cloud-to-ground discharges usually consist of two half cycles. The first half cycle is larger in amplitude and shorter in duration than the corresponding values of the second half cycle. Variations in amplitude and duration of the first and second half cycles were the basis of selecting the various groups in section 3.1. In the following presentations, atmospherics in groups 1 and 2, the normal atmospherics, are represented by circles ( $\circ$ ), atmospherics in groups 3 and 4 by dots ( $\bullet$ ), and group 5 atmospherics by crosses ( $\times$ ). The straight lines, drawn by eye through the data points, represent the relationships between each of the two parameters for the normal atmospherics only.

The distributions of the data points for the normal atmospherics in figures 8, 11, and 14 exhibit relatively good correlations. Fitting the line by least squares or some other more complex method would not necessarily increase usefulness of these data. The same is true for the lines drawn in figures 9 and

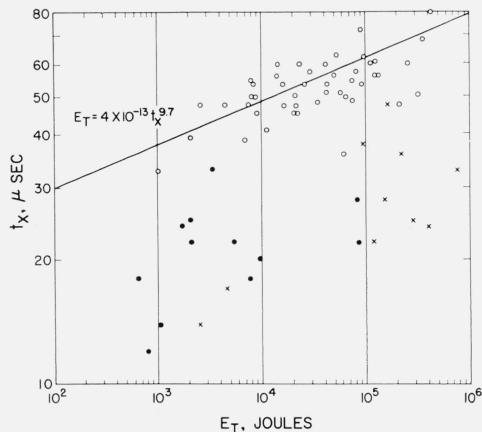


FIGURE 9. First half cycle time versus total radiated energy.

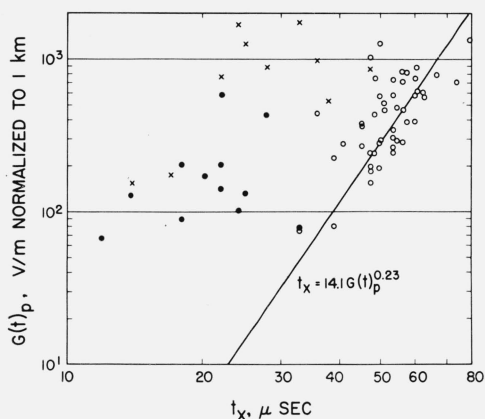


FIGURE 10. Pulse amplitude versus first half cycle time.

10 although the data points are quite scattered. The accuracies of the lines presented in figures 12, 13, and 15 are questionable because of the large scatter of data points. However, for purposes of this study, a line was drawn through the data points in figure 13, and then assuming this was correct, the relationships in figures 12 and 15 were computed. Thus, the relationship between the parameters in figure 12, for example, was computed from the relationships in figures 11 and 13. This was not necessarily the best method, but because of the large scatter of data in figures involving the spectral peak frequency,  $f_0$ , no substantial improvement in the significance or usefulness of these relationships would have been realized through the use of a more sophisticated method. A much larger sample of data would be necessary to improve the accuracies of these three relationships. Therefore, caution should be exercised in attempting to utilize the relationships involving  $f_0$ , presented here, for other related studies.

The pulse amplitude versus total radiated energy is shown in figure 8. The pulse amplitude in volts per meter is the maximum instantaneous value of the radiation field,  $G(t)_p$ , determined from each re-

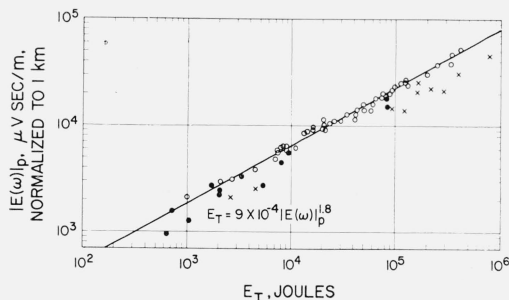


FIGURE 11. Peak spectral amplitude versus total radiated energy.

corded waveform and normalized to 1 km. This normalization was performed by applying ground-wave propagation correction factors to the pulse amplitude depending on the propagation distance and the frequency peak of each spectrum. This is an approximation used for purposes of this report to relate the principal VLF components in the waveform to a common distance. There is a close relationship between these parameters as would be expected from (5) and (6). The straight line drawn through the data points relates total radiated energy to the 2.2 power of the pulse amplitude or peak field strength of the radiation field at 1 km. Atmospherics with longer than average pulse lengths and with higher than average second half cycle amplitudes will plot to the right of the line drawn through the average of the normal type atmospherics.

The relationship between the first half cycle time and the total radiated energy is shown in figure 9. The first half cycle time,  $t_x$  in microseconds, often referred to as the length of the first half cycle, was determined by measuring the time between the initial rise of the groundwave waveform and the point where the waveform crosses the zero axis. This point corresponds to approximately the time when the current moment reaches a maximum. The first half cycle time increases as the total radiated energy increases, but this is not a very close relationship. For other type atmospherics, represented by dots and crosses, the distribution on the graph is very irregular but in general the first half cycle time is much shorter for a corresponding total radiated energy than for the normal type.

Figure 10 shows the relation between the pulse amplitude,  $G(t)_p$  in volts per meter normalized to 1 km, and the first half cycle time,  $t_x$  in microseconds. The relationship is not very strong, but indicates the first half cycle time tends to increase as the pulse amplitude increases. The first half cycle times for other atmospherics are much less than for normal atmospherics at corresponding values of pulse amplitudes.

The spectral peak versus total radiated energy is shown in figure 11. This spectral peak is the maximum value of the amplitude spectrum  $|E(\omega)_p|$  in microvolts seconds per meter, normalized to a distance of 1 km. The normalization includes groundwave attenuation as indicated in section 3.2.

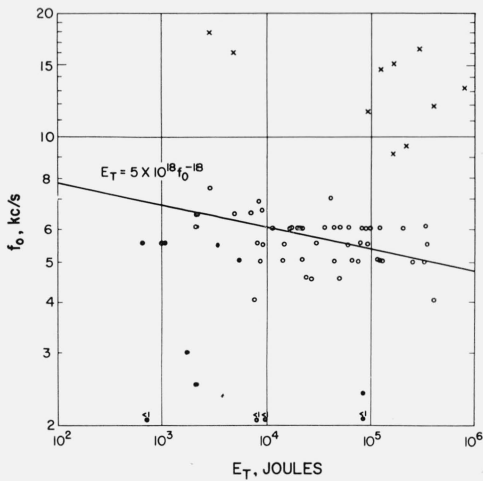


FIGURE 12. Spectral peak frequency versus total radiated energy.

A close relationship exists between these parameters as would be expected since

$$E_T \propto \int_0^{\infty} |E(\omega)|^2 d\omega. \quad (7)$$

The line through the normal type atmospherics relates total radiated energy to the 1.8th power of the maximum amplitude of the spectrum. Other type atmospherics tend to have greater total radiated energy than the normal type atmospherics for a corresponding spectral amplitude. This is understandable since the other type atmospherics are characterized by a shorter pulse length, figure 9, and therefore a broader spectrum than the normal type atmospherics. A broad spectrum contains greater energy than a narrow spectrum for a corresponding value of the maximum spectral amplitude.

The relationship between the spectral peak frequency and the total radiated energy is shown in figure 12. The spectral peak frequency,  $f_0$  in kilocycles per second, is the frequency at which the amplitude spectrum reaches the maximum value. The relation is very poor but indicates in a general way that the spectral peak frequency decreases as the total radiated energy increases for normal type atmospherics. Group 3 and 4 atmospherics, dots, have a lower spectral peak frequency, and group 5 atmospherics, crosses, have a much higher spectral peak frequency than normal type atmospherics for a corresponding total radiated energy value.

Figure 13 shows the relation between the spectral peak and the spectral peak frequency. The relationship between these parameters is not very strong, but indicates that the peak frequency of normal atmospherics tends to decrease as the spectral amplitude increases. The spectral peak frequencies are lower for atmospherics in groups 3 and 4, and are higher for atmospherics in group 5 than for the normal atmospherics group.

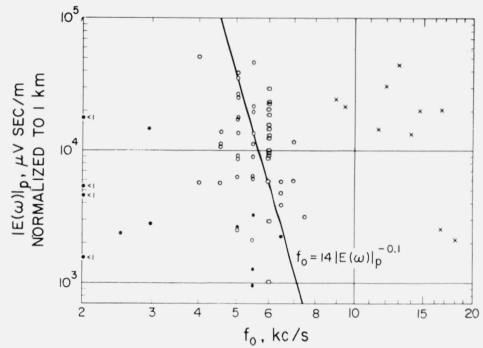


FIGURE 13. Peak spectral amplitude versus spectral peak frequency.

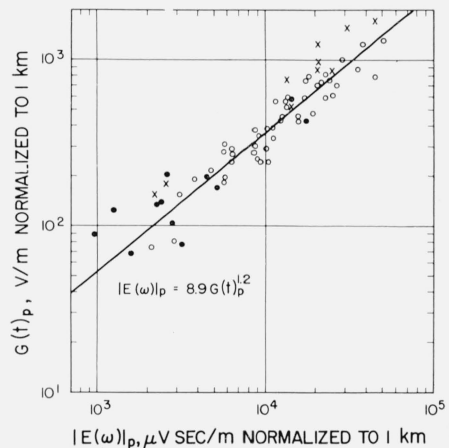


FIGURE 14. Pulse amplitude versus peak spectral amplitude.

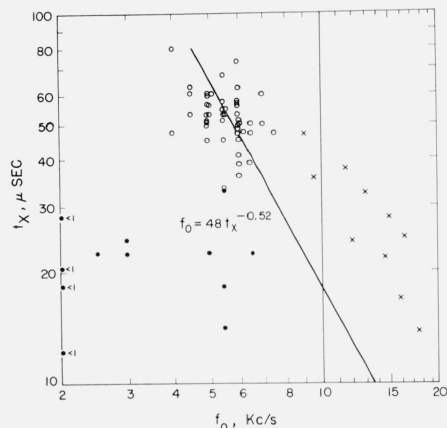


FIGURE 15. First half cycle time versus spectral peak frequency.

A reasonably good relationship is found between the pulse amplitude and the spectral peak as shown in figure 14. This is expected since a larger waveform amplitude produces correspondingly a larger spectral amplitude as indicated in (1).

The first half cycle time versus the spectral peak frequency is shown in figure 15. The relationship is very poor. Group 3 and 4 atmospherics, dots, are scattered over the lower left of the graph; i.e., short first half cycles times and low spectral peak frequencies. Atmospherics in group 5, crosses, are characterized by spectral peak frequencies higher than for the normal type atmospherics. The group 5 data points are reasonably well situated along an imaginary line parallel to the line drawn through the normal atmospherics which indicated that the spectral peak frequency is approximately inversely proportional to the square root of the first half cycle time.

It would be extremely difficult to determine the relationships indicated by the straight line drawn through the normal atmospherics data points as shown in figure 15. This line was computed from the relationships found from the data presented in figures 9 and 12 and by solving for  $f_0$  spectral peak frequency, in terms of  $t_x$ , first half cycle time.

#### 4. Concluding Remarks

An analyses summary giving the average values of each parameter for the various groups is presented in table 2.

TABLE 2. *Analyses summary.*

GROUP	TOTAL ANALYZED	$E_T$ JOULES	$f_0$ , kc/s	$ E(\omega) _p$ $\mu$ v sec/m	$t_x$ $\mu$ sec	$G(t)_p$ v/m
1	36	59,100	5	13,100	53	490
2	11	97,000	5	20,500	53	460
3	8	22,100	$\leq 1$	6,300	20	210
4	4	6,600	$\leq 1$	4,800	23	160
5	10	225,900	12	18,700	28	920
1&2	47	69,100	5	14,800	53	483
3&4	12	16,900	$\leq 1$	5,600	21	192

The normal type atmospherics, represented by groups 1 and 2, have an average total radiated energy of about 69,000 j and a spectral peak at about 5 kc/s. These values represent about 86 percent of all atmospherics within a distance of 500 km of the recording site, and are the primary source of interference at close ranges; i.e., less than 2,000 km. However, at great ranges, the dominant waveguide mode of propagation is characterized by minimum attenuation near 15 kc/s [Chapman and Macario, 1956; Obayashi, Fujii, and Kidokoro, 1959; Taylor and Lange, 1959; Taylor, 1960a, 1960b; Wait, 1957a, 1957b, 1958b]. At 5 kc/s, the attenua-

tion may be 4 to 12 db/1000 km greater than at 15 kc/s, depending on path conditions. Therefore these atmospherics will be greatly attenuated over long distances.

Atmospherics in groups 3 and 4 are characterized by small total radiated energies, about 17,000 j, and a spectral peak near 1 kc/s or less. These atmospherics will be severely attenuated at great ranges.

The group 5 atmospherics have an average spectral peak near 12 kc/s and total radiated energy of about 226,000 j. These atmospherics will propagate to great distances with much less attenuation than experienced by the other groups. From these results, it can be concluded that the group 5 type atmospherics will become statistically more important at great ranges. If amplitude threshold triggering is employed for recording atmospherics from great ranges, all of type 5 will likely trigger the equipment, many of types 1 and 2 will be below the trigger level, and possibly all of types 3 and 4 will be below the threshold.

The eight relationships determined from the data presented in figures 8 through 15 are listed below for convenience:

$$E_T = 5 \times 10^{-2} G(t)_p^{2.2} \quad (8)$$

$$E_T = 4 \times 10^{-13} t_x^{9.7} \quad (9)$$

$$t_x = 14.1 G(t)_p^{0.23} \quad (10)$$

$$E_T = 9 \times 10^{-4} |E(\omega)|_p^{1.8} \quad (11)$$

$$E_T = 5 \times 10^{18} f_0^{18} \quad (12)$$

$$f_0 = 14 |E(\omega)|_p^{-0.1} \quad (13)$$

$$|E(\omega)|_p = 8.9 G(t)_p^{1.2} \quad (14)$$

$$f_0 = 48 t_x^{-0.52} \quad (15)$$

The results presented here are particularly important in the various areas where atmospherics produce a very serious interference problem. It should be possible, with this information, to improve methods that will discriminate against interference from the radiation field of lightning discharges.

The use of atmospherics in VLF propagation studies has become important in recent years because of the application of this band to communication, timing standards, and navigation. Atmospherics are the only readily available signals at frequencies below about 15 kc/s, the lowest frequency commonly available from continuous wave communication emissions; or below about 10 kc/s, the lowest frequency normally used in the Radux-Omega navigational system. Many workers, particularly in England, have reported VLF propagation characteristics from single station recordings for example [Chapman and Macario, 1956; Chapman and Pierce, 1957a; Morrison, 1953]. These workers relied upon an assumed constancy of the radiation spectrum of atmospherics. In view of the results presented here,

that practice is hardly justified and unless extreme care is exercised in the selection of data for such work, erroneous conclusions may result.

Previous work of Taylor and Jean [1959] utilized atmospheric originating in the mountainous regions of Colorado and Wyoming. The cloud-to-ground strokes, for that study, occurred over ground of poor conductivity, i.e.,  $\sigma \leq 10^{-3}$ , and at elevations of 6,000 ft above sea level or higher. The average total radiated energy was about 27,000 j. The present study involved analyzing a larger number of atmospheric than was previously possible and using the waveforms recorded from cloud-to-ground strokes occurring in the Texas and Oklahoma area. In this case, the strokes were over ground of good conductivity, i.e.,  $\sigma \geq 10^{-2}$ , and at elevations of about 1,000 ft above sea level. The average total radiated energy for the "normal" atmospheric was found to be about 69,000 j. It is indicated from these studies that topographical factors, such as ground conductivity and elevation, do control, at least in part, the characteristics of atmospheric.

The author thanks C. L. Alley, University of Utah at Salt Lake City; W. A. Cornell, Stanford University at Palo Alto, Calif.; C. J. Chilton, NBS at Boulder, Colo.; S. Katahara, NBS at Maui, Hawaii; and J. E. Weaver, NBS at Lone Wolf, Okla., for assisting in the collection of data for this paper. Thanks also are due to Dr. H. H. Howe who devised the program for the spectra computations and to L. A. Pollock for tabulating and computing the results and preparing the illustrations. Also, sincere thanks to Dr. H. L. Jones, Oklahoma State University at Stillwater, Okla., for furnishing DF and radar information to aid in determining accurate locations of individual discharges.

## 5. References

- Chapman, F. W., and R. C. V. Marcario (1956), Propagation of audiofrequency radio waves to great distances, *Nature* **177**, 930.
- Chapman, J., and E. T. Pierce (1957a), Relations between the character of atmospheric and their place of origin, *Proc. IRE* **45**, 804.
- Helliwell, R. A., A. G. Jean, and W. L. Taylor (1958), Some properties of lightning impulses which produce whistlers, *Proc. IRE* **46**, 1760.
- Hepburn, F. (1959), Interpretation of smooth type atmospheric waveforms, *J. Atmos. and Terrest. Phys.* **14**, 262.
- Johler, J. R., W. J. Kellar, and L. C. Walters (June 1956), Phase of the low radiofrequency groundwave, *NBS Circ.* **573**.
- Jordan, E. C. (1950), *Electromagnetic waves and radiating systems*, pp. 617, Prentice-Hall Electrical Engineering Series (Prentice-Hall, New York, N.Y.).
- Kitagawa, N., and M. Brook (1960), A comparison of intra-cloud and cloud-to-ground lightning discharges, *J. Geophys. Res.* **65**, 1189.
- Lutkin, F. E. (1939), The nature of atmospheric, *Proc. Roy. Soc.* **171**, 285.
- Malan, D. J., and B. F. J. Schonland (1951), The electrical processes in the intervals between the strokes of a lightning discharge, *Proc. Roy. Soc.* **206**, 145.
- Morrison, R. B. (1953), The variation with distance in the range 0-100 km of atmospheric waveforms, *Phil. Mag.* **44**, 980.

- Norinder, H. (1952), Variations of the electric field in the vicinity of lightning discharges, *Arkiv Geofysik*, **1**, 543.
- Norinder, H., and E. Knudsen (1961), Recent results in the investigation of the relation between lightning discharges and whistlers, *Planet. Space Sci.* **5**, pp. 46 (Pergamon Press, London-New York, N.Y.).
- Obayasky, T., S. Fujii, and T. Kidokoro (1959), An experimental proof of the mode theory of VLF ionospheric Propagation, *J. of Geomag. Geoelec.* **10**, 47.
- Pierce, E. T. (1955a), Electrostatic field-chances due to lightning discharges, *Quart. J. Roy. Meteorol. Soc.* **81**, 211.
- Pierce, E. T. (1955b), The development of lightning discharges, *Quart. J. Roy. Meteorol. Soc.* **81**, 229.
- Taylor, W. L. (1960a), Daytime attenuation rates in the very low frequency band using atmospheric, *J. Research NBS* **64D** (Radio Prop.), No. 1, 349-355.
- Taylor, W. L. (1960b), VLF attenuation for east-west and west-east daytime propagation using atmospheric, *J. Geophys. Res.* **65**, 1933.
- Taylor, W. L., and A. G. Jean (1959), Very-low-frequency radiation spectra of lightning discharges, *J. Research NBS* **63D** (Radio Prop.), No. 2, 199-204.
- Taylor, W. L., and L. J. Lange (1959), Some characteristics of VLF propagation using atmospheric waveforms, *Recent Advances in Atmospheric Electricity*, p. 609 (Pergamon Press, London-New York, N.Y.).
- Wait, J. R. (1957a), The transient behavior of the electromagnetic groundwave over a spherical earth, *IRE Trans. PGAP*, **AP-5**, 198.
- Wait, J. R. (1957b), On the mode theory of VLF ionospheric propagation, *Geofis. Pura e Appl.* **37**, 103.
- Wait, J. R. (1958b), Propagation of VLF pulses to great distances, *J. Research NBS* **61**, No. 3, 187-203.
- Wait, J. R., and H. H. Howe (May 1956), Amplitude and phase curves for groundwave propagation in the band 200 cycles per second to 500 kilocycles, *NBS Circ.* **574**.

## 6. Additional References

- Al'pert, Ia. L., and S. V. Borodina (1959), On the velocity of propagation of electromagnetic waves, *Radiotekhn i Elektron.* **2**, 195.
- Barlow, J. S., G. W. Frey, Jr., and J. B. Newman (1954), Very low frequency noise power from the lightning discharge, *J. Franklin Inst.* **258**, 187-203.
- Bowe, P. W. A. (1951), The waveforms of atmospheric and the propagation of very low frequency radio waves, *Phil. Mag.* **42**, 121.
- Brook, M., and N. Kitagawa (1960a), Some aspects of lightning activity and related meteorological conditions, *J. Geophys. Res.* **65**, 1203.
- Brook, M., and N. Kitagawa (1960b), Electric-field changes and the design of lightning-flash counters, *J. Geophys. Res.* **65**, 1927.
- Bruce, C. E. R., and R. H. Golde (1941), The lightning discharge, *J. Inst. Elec. Engrs. (London)* **88**, 487.
- Caton, P. G. F., and E. T. Pierce (1952), The waveforms of atmospheric, *Phil. Mag.* **43**, 393.
- Chapman, J., and E. T. Pierce (1957b), Les types d'ondes, les spectres de fréquence et la propagation des atmosphériques, *L'onde Electrique*, **362**, 523.
- Crichlow, W. Q. (1957), Noise investigation at VLF by the National Bureau of Standards, *Proc. IRE* **45**, 778.
- Hill, E. L. (1957a), Electromagnetic radiation from lightning strokes, *J. Franklin Inst.* **263**, 107-119.
- Hill, E. L. (1957b), Very low-frequency radiation from lightning strokes, *Proc. IRE* **45**, 775.
- Hopkins, H. G., and B. G. Pressey (1958), Current direction-finding practice, *Proc. IEE* **105**, 307.
- Horner, F. (1954), The accuracy of the location of sources of atmospheric by radio direction-finding, *Proc. Inst. Elec. Engr.* **101**, 383.
- Horner, F. (1958), The relationship between atmospheric radio noise and lightning, *J. Atmos. and Terrest. Phys.* **13**, 140.
- Horner, F., and C. Clarke (1958), Radio noise from lightning discharges, *Nature*, **181**, 688.

- Ishikawa, H., M. Takagi, and T. Takeuti (1958), On the leader waveforms of atmospherics near the origins, *Proc. Res. Inst. Atmospherics (Nagoya Univ.)* **5**, 1.
- Jean, A. G., W. L. Taylor, and J. R. Wait (1960), VLF phase characteristics deduced from atmospheric waveforms, *J. Geophys. Res.* **65**, 907.
- Johler, J. R. (1957), Propagation of the radiofrequency groundwave transient over finitely conducting plane earth, *Geofis. Pura Appl.* **37**, 116.
- Johler, J. R. (1958), Transient radiofrequency groundwaves over the surface of a finitely conducting plane earth, *J. Research NBS*, **60**, (Radio Prop) No. 4, 281-285.
- Johler, J. R., and L. C. Walters (1959), Propagation of a groundwave pulse around a finitely conducting spherical earth from a damped sinusoidal source current, *IRE Trans. PGAP* **AP-7**, 1.
- Jones, H. L. (1959), The identification of lightning discharges by sferic characteristics, *Recent Advances in Atmospheric Electricity*, pp. 543, (Pergamon Press, London, England-New York, N.Y.).
- Kasemir, H. W. (1959), A simple thunderstorm warning device. U.S. Army Signal Research and Development Laboratory, Technical Report 2046, Fort Monmouth, N.J.
- Laby, T. H., J. J. McNeill, F. G. Nicholls, and A. F. B. Nickson (1940), Waveform, energy and reflection by the ionosphere, of atmospherics, *Proc. Roy. Soc.*, **174**, 145.
- Levy, B. R., and J. B. Keller (1958), Propagation of electromagnetic pulses around the earth, *IRE Trans. PGAP* **AP-6**, 56.
- Malan, D. J. (1956), The relation between the number of strokes, stroke intervals and the total durations of lightning discharges, *Geofis. Pura Appl.* **34**, 224.
- Nakai, T. (1960), The study of the amplitude probability distribution of atmospheric radio noise, *Proc. Res. Inst. Atmospherics (Nagoya Univ.)* **7**, 12.
- Norinder, H., and E. Knudsen (1959), Combined analysis of daylight photographs of lightning paths and simultaneous oscillographic records, *Recent Advances in Atmospheric Electricity*, p. 609 (Pergamon Press, London).
- Norinder, H., E. Knudsen, and B. Vollmer (1959), Multiple strokes in lightning channels, *Recent Advances in Atmospheric Electricity*, p. 525 (Pergamon Press, London-New York, N.Y.).
- Pierce, E. T. (1960), Atmospherics from lightning flashes with multiple strokes, *J. Geophys. Res.* **65**, 1867.
- Sao, K. (1960), Researches in the frequency analyses of waveforms of atmospherics—II, *Proc. Res. Inst. Atmospherics (Nagoya Univ.)* **7**, 7.
- Takagi, H., H. Ishikawa, and Takeuti (1959), On the structures of flashes and atmospherics accompanied by cloud discharges, *Pres. Res. Inst. Atmospherics (Nagoya Univ.)* **6**, 1.
- Takeuti, T., H. Ishikawa, and M. Takagi (1960), On the cloud discharge preceding the first ground stroke, *Proc. Res. Inst. Atmospherics (Nagoya Univ.)* **7**, 1.
- Wait, J. R. (1956), Transient fields of a vertical dipole over homogeneous curved ground, *Can. J. Res.* **34**, 27.
- Wait, J. R. (1957c), The attenuation vs frequency characteristics of VLF radio waves, *Proc. IRE* **45**, 768.
- Wait, J. R. (1958a), On the theory of propagation of electromagnetic waves along a curved surface, *Can. J. Phys.* **36**, 9.
- Watt, A. D., and Maxwell (1957), Characteristics of atmospheric noise from 1 to 100 kc, *Proc. IRE* **45**, 787.
- Workman, E. J., M. Brook, and N. Kitagawa, Lightning and charge storage, *J. Geophys. Res.* **65**, 1513.
- Zetrover, W. F., and W. J. Kessler (1951), A note on the similarity of certain atmospherics waveforms, *J. Franklin Inst.* **252**, 137.

(Paper 67D5-286)